HHS Public Access

Author manuscript

*Acta Biomater*. Author manuscript; available in PMC 2016 September 15.

Published in final edited form as:

*Acta Biomater*. 2015 September 15; 24: 53–63. doi:10.1016/j.actbio.2015.06.004.

# Pendant Allyl Crosslinking as a Tunable Shape Memory Actuator for Vascular Applications

**Timothy C. Boire**[#†], **Mukesh K. Gupta**[#†], **Angela L. Zachman**[†], **Sue Hyun Lee**[†], **Daniel A. Balikov**[†], **Kwangho Kim**[‖], **Leon M. Bellan**[†,ξ], and **Hak-Joon Sung**[†,*]

† Department of Biomedical Engineering, Vanderbilt University, Nashville, TN, 37235, United States

‖ Institute of Chemical Biology, Nashville, TN, 37235, United States

ξDepartment of Mechanical Engineering, Vanderbilt University, Nashville, TN, 37235, United States

# These authors contributed equally to this work.

## Abstract

Thermo-responsive shape memory polymers (SMPs) can be fit into small-bore incisions and recover their functional shape upon deployment in the body. This property is of significant interest for developing the next generation of minimally-invasive medical devices. To be used in such applications, SMPs should exhibit adequate mechanical strengths that minimize adverse compliance mismatch-induced host responses (e.g. thrombosis, hyperplasia), be biodegradable, and demonstrate switch-like shape recovery near body temperature with favorable biocompatibility. Combinatorial approaches are essential in optimizing SMP material properties for a particular application. In this study, a new class of thermo-responsive SMPs with pendant, photocrosslinkable allyl groups, x%poly( -caprolactone)-co-y%( -allyl carboxylate -caprolactone) (x%PCL-y%ACPCL), are created in a robust, facile manner with readily tunable material properties. Thermomechanical and shape memory properties can be drastically altered through subtle changes in allyl composition. Molecular weight and gel content can also be altered in this combinatorial format to fine-tune material properties. Materials exhibit high elastic, switch-like shape recovery near 37 °C. Endothelial compatibility is comparable to tissue culture polystyrene (TCPS) and 100%PCL *in vitro* and vascular compatibility is demonstrated *in vivo* in a murine model of hindlimb ischemia, indicating promising suitability for vascular applications.

[*]**Corresponding Author**hak-joon.sung@vanderbilt,edu. Tel.: 1-615-322-6986..



Appendix A. Supplementary data

Synthetic scheme, $^{1}$H-NMR spectra of 100%PCL-dimethacrylate, and shape memory video demonstration.

**Keywords**

Allylic compounds; shape memory polymers; thermally responsive materials; structure-function relationships; biocompatibility

## 1. Introduction

Shape memory polymers (SMPs) contain chemical and/or physical crosslinks that afford the ability to be programmed and fixed into a temporary shape until provoked by a specific external stimulus to recover their original, permanent shape [1]. A diverse array of SMPs have been developed that recover their permanent shape in response to light [2], magnetic fields [3], electricity [4], moisture [5], or pH [6] for a variety of industrial, aeronautical, and biomedical applications and can be reviewed elsewhere [1, 7, 8]. In contrast to their shape memory alloy counterparts, SMPs can be created with diverse, multi-functional chemistries to enable drastic yet highly-controllable shape responses to various stimuli [9-12]. SMPs that are thermo-responsive remain the most convenient and widely studied, drawing extensive interest in the biomedical field in part because of the high predictability and consistency of the body temperature stimulus [1, 13-15]. The capability of thermo-responsive SMPs to recover their permanent shape near body temperature after programming into a distinct temporary shape provides an opportunity to develop the next generation of minimally-invasive medical devices [1, 13-15]. For example, their temporary shape can be programmed to fit through a small-bore incision for catheter insertion at room temperature and, when heated at or near body temperature, the polymeric device recovers its original functional shape, such as a stent mesh for intraluminal expansion [15-17], an expandable foam to fill an aneurysm [18-20], a tubular graft to bypass bloodflow in the advent of minimally invasive bypass grafting procedures [21], or a corkscrew shape to remove endovascular blood clots [22-24].

To be used in such vascular applications, materials should exhibit mechanical strengths that accomplish intended functions and minimize adverse compliance mismatch-induced host responses [25-28], be biodegradable to prevent infectious complications [29-32], and demonstrate switch-like shape recovery near body temperature [32, 33] with favorable biocompatibility [34-36]. SMPs triggered by melting temperature ($T_m$) may be more appropriate for many biomedical applications because they tend to exhibit sharper phase transitions and higher, more switch-like shape recovery than SMPs that respond to glass transition temperature ($T_g$) [32, 37]. Moreover, covalently-crosslinked SMP networks are often preferable to physically-crosslinked ones because they tend to undergo less creep and irreversible deformation during programming steps [1, 38], exhibiting superior shape memory properties and thermal stability [39]. However, current approaches to synthesize $T_m$-triggered SMP thermosets require an additional methacrylate functionalization step or multistep monomer synthesis [33, 40, 41].

In this study, a new class of $T_m$-responsive SMPs with pendant, photocrosslinkable allyl groups, x%poly( -caprolactone)-co-y%( -allyl carboxylate -caprolactone) (x%PCL-y %ACPCL), are created in a robust, facile manner with readily tunable material properties.

While $T_g$-triggered SMPs have been created via thiol-ene crosslinking between monomers containing thiol and allyl groups [42] or via pendant crosslinking of acrylate groups [43], this is the first study to create SMPs by photocrosslinking pendant allyl groups. The x %PCL-y%ACPCL copolymerization format offers a convenient, combinatorial approach to fine-tune material properties of SMPs. The pendant allyl carboxylate-based crosslinkers enable pendant conjugation to growth factors, therapeutics, and extracellular matrix-derivatives via thiol-ene click chemistry [44, 45] or photocrosslinking of modified peptides [46] to control cell and tissue responses. Allyl composition (y%) can be used to simultaneously control both the spacing of netpoints and crystallinity, offering an efficient means to tune thermomechanical, shape memory, and biological functions. Further tweaking of material properties and functions can be attained by altering other physicochemical properties such as molecular weight and gel content. Therefore, the new copolymerization format provides a unique, finely-tunable platform for studying structure-function relationships in order to better control biological responses and meet application requirements [47].

PCL notably has many desirable properties for vascular applications including biocompatibility/bioresorbability, slow biodegradability (2 – 3 years *in vivo*), and mechanical compliance [48], but its $T_m$ (> 50 °C) is too high for physiological applications. Previous efforts to lower its $T_m$ near 37 °C and achieve either dual- or triple-shape memory functions involve incorporation or complexation of rigid and/or soft components, blending, branching, and molecular weight alteration [33, 40, 41, 49-54]. In this study, the $T_m$ is tuned near body temperature primarily through subtle alteration in the molar composition of x %PCL-y%ACPCL. This new pendant-crosslinking system with photocrosslinkable ally-based crosslinkers offers the advantages of facile fabrication, robust tunability of material properties, and further functionalization with bioactive molecules. Molecular weight and gel content can also be controlled in this copolymerization format to fine-tune properties such as mechanical compliance and extensibility to more closely match that of the native artery, in turn reducing thrombotic and restenotic risks [14, 28, 48, 55]. These SMPs exhibit exceptional shape memory properties with high elastic recovery and switch-like shape responses near 37 °C. In addition, these SMPs are compatible with vascular endothelial cells (ECs), as indicated by high levels of cell viability (• 85% after 91 hours relative to tissue culture polystyrene (TCPS)) and healthy cell morphologies. Vascular compatibility (i.e. successful cellularization without inflammatory exacerbation) is also shown *in vivo* in a murine model of hindlimb ischemia. These material features (e.g. high elastic recovery, ease of manufacturing and programming, low cost, vascular compatibility, tunable material properties, mechanical compliance, and biodegradability) are advantageous towards minimally invasive deployment of bulky, complex implantable devices for various biomedical applications [13-15], such as the aforementioned intraluminal stents, bypass grafts, or clot removal devices.

## 2. Experimental

### 2.1 Materials

Lithium diisopropyl amine (LDA), allyl chloroformate, anhydrous tetrahydrofuran (THF), diethylzinc solution (15 wt% in toluene), dichloromethane (DCM), ethyl acetate, hexanes, poly(vinyl alcohol) (PVA), and ethanol were used as purchased from Sigma-Aldrich (St. Louis, MO). ε-caprolactone (CL) was dried with calcium hydride and vacuum distilled. To purify the synthesized α-allyl carboxylate ε-caprolactone (ACCL), Silica Gel Premium Rf (Sorbent Technologies, Norcross, GA) was first loaded into a glass column and wetted with 100% hexanes. Poly(methyl methacrylate) (PMMA) standards (Agilent Technologies, Inc., Santa Clara, CA) were used as purchased. SYLGARD® 184 Silicone Elastomer Kit (Dow Corning, Inc., Midland, MI) was used to prepare polydimethylsiloxane (PDMS) molds for preparing SMP shapes. MesoEndo Endothelial Cell Growth Media (Cell Applications, Inc., San Diego, CA) was used as purchased with passage 5-cultured human umbilical vein endothelial cell (HUVEC) and human coronary artery endothelial cell (hCAEC) lines (Cell Applications, Inc., San Diego, CA). Resazurin sodium salt (Sigma-Aldrich) was further diluted from prepared sterile 5 mM stock aliquots. Ethidium Homodimer-1 and Alexa Fluor® 488 Phalloidin were used as purchased (Molecular Probes, Eugene, OR). For animal experiments, 5-0 Prolene sutures (Ethicon, Somerville, NJ) and optimal cutting temperature compound (OCT, Sakura Finetek USA, Inc., Torrance, CA) were used as purchased.

### 2.2 Synthesis of ACCL monomer

Analogous to other works [56-58], distilled CL (13.9 mL, 125 mmol) was added dropwise to a 250 mL round-bottom flask containing LDA (125 mL of 2 M in THF/n-heptane/ethylbenzene, 250 mmol) in anhydrous THF (200 mL) at −78 °C. After 1 hour, the temperature was raised to −30 °C and allyl chloroformate (13.3 mL, 125 mmol) was added dropwise. Thirty minutes later, the temperature was raised to 0 °C and quenched with saturated $NH_4Cl$ (30 mL). The crude ACCL was diluted in $H_2O$ (100 mL), extracted with ethyl acetate (300 mL × 3), dried with $Na_2SO_4$, filtered, evaporated, and purified by column chromatography using Silica Gel Premium Rf (Sorbent Technologies) with 10% ethyl acetate in hexanes to yield the novel monomeric compound (58% yield, 14.3 g, 72 mmol).

### 2.3 Synthesis of x%PCL-y%ACPCL copolymers

Analogous to other works [56, 59], varying molar ratios of dried ACCL and CL (100 mmol total) were introduced to a pre-dried test tube containing 1,6-hexanediol (0.5 mmol). The polymerization mixture was degassed with two freeze-purge-thaw cycles, submerged in a 140 °C oil bath, and catalyzed with dropwise addition of $Zn(Et)_2$ (1 mmol, 15 wt% in toluene) for 1 hour. The solution was precipitated in cold diethyl ether and dried under vacuum to yield the novel polymeric compound.

### 2.4 Fabrication of crosslinked x%PCL-y%ACPCL and 100%PCL-dimethacrylate SMP Films

Films of uniform thickness (~0.3 mm) were produced from a DCM solution (10 wt% polymer, 1 wt% 2,2-dimethoxy-2-phenylacetophenone) via a thin film applicator (Precision Gage & Tool, Co., Dayton, OH) and 365 nm irradiation (4.89 J $cm^{-2}$, 18.1 mW $cm^{-2}$, 4

min) with a Novacure 2100 Spot Curing System (Exfo Photonic Solutions, Inc., Mississauga, Ontario, Canada). Films were then solvent casted and vacuum dried.

### 2.5 Characterization of monomer, polymers, and crosslinked SMP films

To characterize molar compositions of compounds, $^1$H-NMR was performed on5 wt% solutions in $CDCl_3$ with a 300 MHz spectrometer (Bruker Instruments, Inc., Billerica, MA). Molecular weight properties were determined by gel permeation chromatography against PMMA standards using a Phenogel 10E3A column (Phenomenex Inc., Torrance, CA) in THF. Polydispersity (PDI) was determined by the $M_w$ / $M_n$ ratio.

To determine gel content, $X_G$, the dry mass of film samples for each composition, $m_{initial}$, was recorded (n = 3 – 4). Following two days of incubation in DCM, samples were extracted, dried, and weighed as $m_{extracted}$ to calculate $X_G$:

$$X_G = m_{extracted}/m_{initial} \times 100\%$$

Thermal properties were determined by subjecting samples (n = 3 – 4) to two cycles from −80 °C to 150 °C on a Q1000 differential scanning calorimeter (DSC) (TA Instruments, Inc., New Castle, DE). $T_m$, crystallization temperature ($T_c$), $T_g$, enthalpy of fusion ($\bullet H_m$), and enthalpy of crystallization ($\bullet H_c$) are reported from the second cycle. Percent crystallinity, $X_C$, is calculated as:

$$X_C = \Delta H_m/\Delta H_m^o \times 100\%, \quad \text{where} \quad \Delta H_m^o = 139.5 \quad \text{J/g}, \quad \text{the enthalpy of fusion for} \quad 100\% \quad \text{crystalline} \quad PCL \quad [60].$$

To determine mechanical and shape memory properties of the SMP films, rectangular strips (~8 mm × ~2.2 mm × ~0.3 mm) were loaded (n = 3 – 4) into a tensile clamp affixed within a dynamic mechanical analyzer (TA Instruments Q2000). Similar to Guo et al. [61], tensile mechanical properties were determined isothermally at 37 °C with a stress ramp of 0.1 MPa $min^{-1}$. The modulus at 37 °C, $E_{tn}$(37 °C), was determined by measuring the slope in the initial linear region of the stress vs. strain curve.

Shape memory properties were determined in controlled force mode by stress-controlled thermomechanical cycling in which shape programming is controlled by stress and strain recovery is recorded under stress-free conditions [61-63]. SMP films were (1) heated to $T_m$ + 15 °C, equilibrated for 10 minutes to achieve the original permanent shape, $_p$(0), and programmed into an elongated shape by subjecting to tensile stress (0.004 MPa $min^{-1}$ to 0.039 MPa), (2) cooled (2 °C $min^{-1}$ to 0 °C) and equilibrated isothermally for 10 minutes at 0 °C to yield the maximum strain, $_1$(N), and (3) relieved of stress (0.004 MPa $min^{-1}$ to 0 MPa) to yield the temporary shape, $_u$(N). (4) Heating (2 °C $min^{-1}$) above $T_m$ yielded the permanent shape, $_p$(N), after a final 10 minute isothermal equilibration step at $T_m$ + 15 °C. Shape recovery, $R_r$(N), describes how well shape is recovered ( $_p$(N)) in comparison to the beginning of the $N^{th}$ cycle ( $_p$(N-1)) after deforming to maximum strain $_1$(N). Shape fixity,

$R_f$(N), defines the ability to maintain programmed shape $_1$(N) after unloading of stress to yield the temporary shape $_u$(N).

$$\mathrm{R_r}\,(\mathrm{N}) = \frac{\varepsilon_1\,(\mathrm{N}) - \varepsilon_\mathrm{p}\,(\mathrm{N})}{\varepsilon_1\,(\mathrm{N}) - \varepsilon_\mathrm{p}\,(\mathrm{N}-1)} \times 100\%; \quad R_f\,(N) = \frac{\varepsilon_u\,(N)}{\varepsilon_1\,(N)} \times 100\%$$

### 2.6 Shape programming

Closed-end polymer tubes (~1.0 – 2.0 cm length, ~0.90 mm in I.D., ~1.0 - 1.6 mm O.D.) were prepared by dipping a polyvinyl alcohol (PVA)-coated 0.90 mm O.D. glass capillary in the polymer film preparatory solution and UV-crosslinking as above. Capillaries containing the tubes were dried and immersed in deionized $H_2O$ and 100% ethanol before manually pulling the tubes off the capillaries. The tubes were washed with $H_2O$, dried, and the open side of the tube was closed by dipping it in polymer solution and UV crosslinking. A guitar shape comprised of 96%PCL-04%ACPCL was prepared by first laser etching (Epilog Laser, Golden, CO) a 2 mm PDMS mold containing a CAD-designed guitar, then pouring the 94%PCL-06%ACPCL polymer solution into the mold and UV crosslinking (365 nm, 26.1 J $cm^{-2}$, 290 mW $cm^{-2}$) on a 48 °C hotplate.

### 2.6 Analysis of structure-function relationships

A 13 × 10 matrix was constructed containing the mean values of each variable to be compared (13 variables) for each of the 10 polymer films. Matrix values were standardized to their z-score for more apt comparison between variables, and a covariance matrix was computed and plotted using MATLAB (MathWorks Inc., Natick, MA). To highlight structure-function relationships and minimize redundancy, only a portion of this matrix is presented.

### 2.7 HUVEC viability

To prevent cell attachment on TCPS underneath test films, wells were coated with 1% agarose solution. Agarose-coated wells were dried, washed with 100% ethanol, UV sterilized, and washed with MesoEndo Endothelial Cell Growth Media. Ethanol-leached, media-soaked polymer disks (~31 $mm^2$, ~50 μm thick) were then placed on the agarose-coated wells, and Passage 5 HUVECs (470 cells $mm^{-2}$) were seeded directly on the film surfaces, TCPS (positive control), and 1% agarose (negative control) (n = 4). After 1.5 hours, 150 μL of media was added. Viability was assessed at 9, 35, and 91 hour time points via the resazurin assay [64]. Briefly, resazurin was added to each well to achieve a 5 μM concentration in MesoEndo, incubated for 4 hours at 37 °C, and 560/590 nm excitation/emission of the supernatant was read on an Infinite® M1000 Pro plate reader (Tecan Group Ltd, San Jose, CA). Viable cell number was calculated based on a standard curve of fluorescence intensity from HUVECs on TCPS, and % cell viability was normalized to TCPS controls. All samples were tested in biological quadruplicates.

### 2.8 HCAEC viability and morphology

Cell viability was assessed for Passage 5 hCAECs seeded on TCPS (380 cells $mm^{-2}$) and subsequently co-incubated with ethanol-leached, media soaked films (n = 4). The resazurin assay was utilized in the same manner as that described above at 24 and 80 hours.

Cell morphology was evaluated by seeding the Passage 5 hCAECs directly onto polymer disks (n = 4). After 3 days on the polymer disks or TCPS controls, cells were fixed with 4% paraformaldehyde (15 minutes), permeabilized with 0.5% Triton X-100 (10 min), and blocked with 10% bovine serum albumin (30 min). Cells were then incubated with 2 μM Ethidium Homodimer-1 (10 min) and 50 μM Alexa Fluor® 488 Phalloidin (20 min). Cells on polymer surfaces were imaged on a LSM 510 META Inverted Confocal Microscope (Carl Zeiss, LLC, Thormwood, NY), while TCPS controls were imaged with a Nikon Eclipse Ti inverted fluorescence microscope (Nikon Instruments Inc. Melville, NY). Images were post-processed and analyzed using ImageJ software (NIH, Bethesda, MD).

### 2.9 In vivo biocompatibilty

All animal experiments were approved by the Vanderbilt Institutional Animal Care and Use Committee (IACUC) in accordance with the NIH Guide for the Care and Use of Laboratory Animals. Wild type A/J mice were used to develop a model of hindlimb ischemia by ligating the femoral artery and vein at one ligation below the epigastric artery and a second ligation around the artery and vein at a distal location just proximal to the deep femoral branch [65-67]. The femoral artery and vein were then cut between these two sutures. Immediately prior to surgery, closed-end tubular SMP scaffolds (0.9 cm I.D., 1.2 cm O.D., 1.5 cm length) comprised of 89%PCL-11%ACPCL were rinsed thoroughly with ethanol, UV sterilized, vacuum dried, and implanted into the thigh muscle adjacent to the femoral artery ligations. The surgical incision was then closed with non-degradable sutures. Following the two week implantation, the tubular SMP scaffolds were harvested and embedded in OCT, frozen at −80 °C for 24 hours, and sectioned (5 μm sections) using a cryotome. To visualize cell infiltration and inflammatory responses as evidence of *in vivo* biocompatibility of SMP scaffolds, sections were H&E stained and imaged on a Nikon Eclipse Ti inverted fluorescence microscope (Nikon Instruments Inc. Melville, NY).

### 2.10 Statistical Analysis

All data are reported as mean ± standard deviation (n = 3 - 4). In comparisons between individual groups, an unpaired, two-tailed Student's t-test was used and $p < 0.05$ was considered statistically significant.

## 3. Results and discussion

### 3.1. Synthesis and characterization of x%PCL-y%ACPCL copolymers

To prepare this new class of SMP library, a novel -allyl carboxylate -caprolactone (ACCL) monomer was first synthesized in a single reaction by lithium diisopropyl amine-mediated carbanion formation at the -carbon of -caprolactone (CL) and subsequent addition of allyl chloroformate (**Figure 1A**) [56, 58]. $^{1}$H-NMR confirmed formation of the desired ACCL product, as indicated by characteristic allyl (5.92 ($\boldsymbol{G_i}$) , 5.31 ($\boldsymbol{H_{ii}}$) and 4.63 ($\boldsymbol{F_{ii}}$) ppm) and

CL peaks (**Figure 1C**) [56, 57, 59, 68]. Ring-opening (co)polymerization (ROP) of ACCL with CL using a diethylzinc catalyst and 1,6-hexanediol initiator generated a library of novel x%PCL-y%ACPCL (*x* and *y*: molar ratio) copolymers with y = 4.16 – 14.5% as determined by the ratio of allylic CH protons ($G_i$, = 5.92 5.92 ppm) to $CH_2$ protons at the -carbon of PCL and ACPCL units ($\varepsilon_{ii}$, = 4.15 ppm) (**Figure 1B and 1D**, **Table 1**) [56, 57, 59, 68]. As a control, 100%PCL [**Table S1**, $M_n$ = 11300 Da, PDI = 1.54] was similarly synthesized by ROP of CL using stannous octoate and terminally-functionalized via reaction with 2-isocyanatoethyl methacrylate to yield 100%PCL-dimethacrylate [100%PCL-DMA, **Table 1**, $M_n$ = 11628 Da, PDI = 1.41] with a terminal hydroxyl-to-methacrylate conversion ($D_M$) of 90.5% (**Figure S1**, **Equation S1**) [38, 69]. Allylic compositions attained were lower than the ACCL:CL feed ratios due to lower reactivity of the ACCL monomer (**Table 1**, **Figure 1E**) [56, 59]. Molecular weight [**Table 1**, $M_n$ = 12 – 19 kDa, polydispersity index (PDI) = 1.78 – 2.50] was controlled by the 1,6-hexanediol initiator: total monomer ratio but was also influenced by the feed ratio of the less reactive ACCL monomer [56, 59]. The higher PDIs and lower yields (22.6 – 56.6%) attained for these copolymers may be due to transesterification reactions involving both the polyester backbone and pendant allyl carboxylates [41, 56, 59]. There is a clear inverse relationship between several thermal properties and allyl composition, as the amorphous ACPCL disrupts PCL crystallinity, lowering the $T_m$ and percent crystallinity ($X_c$) (**Table 1**).

### 3.2. Fabrication and characterization of crosslinked x%PCL-y%ACPCL SMP networks

A subset of x%PCL-y%ACPCL copolymers and the 100%PCL-DMA control were photocrosslinked to create the shape memory effect and evaluated in terms of gel content, thermal, mechanical, and shape memory properties. It was desired to produce SMPs with $T_m$'s both slightly above and below 37 °C as surgical preferences for the onset of shape recovery depend on the particular application [15, 70, 71]. In order to be used for various vascular applications (e.g. endovascular stents, bypass grafts), it was also desired that the SMP library exhibits tunable mechanical properties, with sufficient compliance and extensibility. Moreover, complete and repeatable shape recovery with an on-off “switch-like” response to small temperature changes is sought after in order to tightly control shape memory behavior and preserve implant integrity and function following shape programming and recovery.

Gel content, which relates to the percent crosslinking of the material, is independent of composition (**Figure 5**, subset) and was an average of 57.3 ± 7.2% for the x%PCL-y %ACPCL films after photocrosslinking (365 nm, 4.89 J $cm^{-2}$, 18.1 mW $cm^{-2}$), well above the 10% [72] or 30% [73] threshold for achieving the shape memory effect in other SMP networks (**Table 2**). Higher gel content films can be achieved for each composition by increasing the UV dosage, but are not included here because they exhibit hindered shape memory functions due to low crystallinity. Crosslinking of the materials resulted in a $T_m$ reduction from 45.9 – 32.5 °C to 43.4 – 29.7 °C for y = 4.16 – 14.5% copolymer films (**Table 1 and 2**) due to the restricted mobility of the crosslinked polymer chains [33, 41, 61]. This reduced chain mobility also disrupts the alignment of chains after melting, as indicated by a reduction in the percent crystallinity ($X_C$) after crosslinking [41]. There is a clear dependence of all thermal properties (except for $T_g$) on molar composition for the

crosslinked polymers (**Table 2**, **Figure 2 and 5**), as amorphous ACPCL disrupts the crystallinity of PCL and simultaneously lowers the $T_m$, $X_C$, crystallization temperature ($T_c$), and enthalpy of crystallization (•$H_c$). Copolymers with > 15%ACPCL follow the same trend, but were not considered for this paper because their low crystallinity inhibits their shape memory utility. The $X_C$ generated is similar to branched PCL crosslinked films [33], indicating that switch-like shape recovery behavior is feasible with these SMPs. Crosslinking produced a library of SMPs with ideal switching temperatures (i.e. $T_m$'s near 37 °C) and sufficient $X_C$ for complete shape recovery and switch-like behavior in physiological applications.

Mechanical properties of the SMP test films were assessed isothermally at 37 °C to determine suitability for vascular applications. The elasticity was of the same order of magnitude or one lower than the 100%PCL-DMA control [**Table 3**, for y = 4.16 – 14.5%: tensile modulus at 37 °C ($E_{tn}$(37°C)) = 70.8 - 2.48 MPa], which may be considered desirable compliance for vascular applications considering that this is only marginally less compliant than arteries [14, 28, 33, 48, 55]. By comparison, healthy human coronary arteries exhibit an average physiological elastic modulus of 1.48 MPa [74]. The higher y%ACPCL crosslinked copolymer films displayed an order of magnitude lower $E_{tn}$(37°C) that more closely matches that of native arteries and is primarily the result of these materials partially or fully melting at 37 °C [33]. Stress-to-break, $_{max}$, exhibits a similar trend as $X_C$, decreasing from 3.15 to 0.46 MPa as y% increased from 4.16 to 14.5%. All materials exhibit good ductility at 37 °C, with >100% strain-to-break, $_{max}$, for every test film but 85%PCL-15%ACPCL ( $_{max}$ = 71.5 ± 40.6%), which may be adversely affected by its low crystallinity (**Table 3**). These experiments demonstrate that the library of crosslinked SMPs has appropriate extensibility and compliance for vascular applications.

Next, their shape memory properties were evaluated by stress-controlled thermomechanical cycling in which shape programming is controlled by stress and strain recovery is recorded under stress-free conditions (**Figure 4A – C**) [61-63]. Some of the SMP films, most notably 96%PCL-04%ACPCL, exhibit shape changes when heated above their $T_m$ for the first time during the equilibration step at $T_m$ + ~15 °C before any stress is applied (i.e. ~39% negative strain at 60 °C **in Figure 4A**). Similar to crosslinked semi-crystalline SMPs utilized in heat-shrink tubing applications [1, 75-77], this indicates that the film fabrication process (i.e. UV irradiating the SMPs below their $T_m$) can effectively fix the films in an ambient temporary shape. Heating beyond their $T_m$ for the first time triggers recovery of an entropically-favored permanent shape, $_p$(0), that may differ from the temporary shape formed during the crosslinking event at room temperature. SMPs should therefore be photocrosslinked above their $T_m$ in the future to avoid any possible unanticipated alterations in the permanent shape. Smaller stresses than those in **Figure 3** are required to achieve comparable levels of strain because the programming step is carried out at temperatures higher than 37 °C ($T_m$ + ~15°C). Shape fixity ($R_f$) represents the ability of materials to be programmed and fixed into a temporary shape (e.g. thread-like shape) and was > 98% for select films of every composition (**Table 3**). This indicates that even less crystalline materials have strong enough interactions between polymer chains [1], at least at freezing temperatures, to properly immobilize and fix a temporary shape. Shape recovery after the first cycle, $R_r$(N), which

indicates the quantitative ability of materials to recover their permanent shape (e.g. tubular shape), was > 98% for test films of every composition except for 85%PCL-15%ACPCL ($R_r(N)$ = 86.9 ± 4.7%) (**Table 3**). The lower $R_r$, $X_C$, and ductility of crosslinked 85%PCL-15%ACPCL films indicate that the lower crystallinity and energy associated with the melting transition of materials with • 15%ACPCL hinders their shape memory utility. The highly repeatable nature of shape programming and recovery for these SMPs with < 15%ACPCL is illustrated in three consecutive thermomechanical cycles with 96%PCL-04%ACPCL and 89%PCL-11%ACPCL along with the 100%PCL-DMA control (**Figure 4A – C**). This indicates their promising utility in biomedical applications involving deployment and recovery from minimally-invasive surgical devices such as catheters or laparoscopes [1, 13-15]. Shape memory demonstrations further affirm this potential capability to be programmed into and recover complex shapes in biomedical applications (**Figure 4D – L**, **Video S1**), including a thread-to-tube transition for possible minimally-invasive catheter/laparoscope deployment in endovascular stenting, bypass grafting, or clot removal at 37 °C. Shape recovery occurs rapidly (within seconds) and fully once the SMPs are exposed to a temperature at or beyond their midpoint $T_m$ (**Video S1**). All copolymers, especially those with < 15% ACPCL, possess exceptional, tightly-controllable shape memory capabilities.

### 3.3. Elucidation of structure-function relationships

To better elucidate correlations of material properties ($T_m$, $H_m$, $T_c$, $E_{tn}$(37°C), $_{max}$, $_{max}$, $R_r(N)$, $R_f(N)$) with physicochemical properties (y%ACPCL, $M_n$, $M_w$, PDI, $X_G$), a standardized covariance matrix was constructed from mean property values of an expanded polymer library (**Figure 5**). Covariances (covs) closest to the absolute value of 1 indicate the strongest correlations between variables, with positive and negative values indicating direct and inverse relations, respectively. While it should be cautioned that the low number of polymer test groups (n = 10), inherent variance in data, interdependent relationships, and experimental parameters used to derive mechanical and shape memory properties (e.g stress or strain rate, fixation and deformation temperature) can skew these correlations, some basic and useful conclusions can be drawn from this analysis. Thermal properties ($T_m$, •$H_m$, $T_c$, •$H_c$), $E_{tn}$(37°C), and $_{max}$ correlate most strongly with y%ACPCL (cov = −0.80 – −0.94), indicating the dominant role of molar composition in modulating thermal properties. The effect of molar composition on many material properties can be explained by the fact that altering allyl content simultaneously changes both the crystallinity and spacing of netpoints of the crosslinked networks. $R_r(N)$ was also most impacted by molar composition (cov = −0.60), although it is conceivable that programming parameters (e.g. fixation and deformation temperature, stress or strain rate) could be adjusted to improve $R_r(N)$ for higher y%ACPCL copolymers [78-80]. Also of note, $M_n$ only correlates strongly with $_{max}$ (cov = 0.78), indicating that increasing $M_n$ may be able to improve the extensibility of these SMPs if that is deemed a rate-limiting factor in implant performance. Along the same lines, it may be possible to increase $R_f(N)$ (cov = −0.54) and •$H_m$ (cov = −0.46) by adjusting $X_G$. While a low number of polymer test groups, variability in the data, interdependencies, and the potential influence of experimental parameters convolute this analysis, it appears that the majority of material properties are most affected by molar composition. Furthermore, it appears that many material properties can be tweaked via modulation of other

physicochemical properties to comprise PCL-ACPCL SMPs with optimal thermal, mechanical, and shape memory properties for a particular application. Firmer conclusions can be derived from these correlations if the polymer library is further expanded, thereby minimizing variance in the data and interdependent effects.

### 3.4. Cell viability studies

To assess biocompatibility of the films *in vitro*, HUVECs were seeded on washed polymer films and their viability was measured and normalized to TCPS over the course of four days using the resazurin assay (**Figure 6A**) [64]. The 85%PCL-15%ACPCL copolymer was not considered for this test due to its lower ductility and shape memory utility. 100%PCL (Sigma-Aldrich, $M_n$ = 70 – 90 kDa) is an appropriate control film as the base polymer of x %PCL-y%ACPCL films and is well known to be biocompatible [35, 81]. Nine hours post-seeding, there was no statistically significant difference in HUVEC viability on test SMP films (60.0 – 65.2% relative to TCPS) compared to 100%PCL (59.4 ± 4.9%), affirming that cell seeding was equivalent across the films. At later timepoints, HUVEC viability on all copolymer films (102.9 – 106.7% for 35 hours and 85.0 – 103.0% for 91 hours) was comparable to that on the TCPS control (100%) and greater than that on 100%PCL (66.0 ± 14.4% and 64.1 ± 32.0%, respectively). hCAECs seeded on TCPS and immediately co-incubated with polymer films exhibited a viability of > 79% at 24 hours and > 85% at 80 hours relative to TCPS, with no statistically significant differences observed between test substrates (n = 4) (**Figure S2**). In a separate experiment, hCAECs seeded directly on films demonstrate a trademark cobblestone morphology indicative of their excellent viability on all films three days post-seeding (**Figure 6B - F**)[82]. These experiments therefore demonstrate that the SMPs are compatible with vascular ECs.

### 3.5. In vivo biocompatibility

The biocompatibility of SMPs was further assessed *in vivo* in terms of cellular infiltration and host inflammatory responses elicited by SMP implantation in a mouse model of hindlimb ischemia. A washed, sterilized tubular SMP scaffold was implanted into the thigh muscle adjacent to the two femoral artery ligations. The 89%PCL-11%ACPCL copolymer was chosen as the tubular construct because it possesses exceptional shape memory properties ($R_f$ and $R_r$ > 99%), a $T_m$ close to body temperature (37.9 °C), and the highest EC biocompatibility after 91 hours (103.0%). A murine model of hindlimb ischemia was chosen because it is a well-established method for inducing ischemic environments commonly encountered by medical devices utilized in vascular applications such as stents and grafts [65-67]. After two weeks, H&E staining of the harvested tubular SMP constructs reveals successful cellularization without inflammatory exacerbation as evidenced by the absence of foreign body giant cell formation or observable fibrotic tissue formation (**Figure 7**). While further long-term *in vivo* studies are required for use in a particular application, this preliminarily result of mild host immune responses and good biocompatibility suggests that SMP constructs are a promising material to address vascular injury in an ischemic environment.

## 4. Conclusions

In conclusion, x%PCL-y%ACPCL crosslinked networks are the first SMPs with crosslinked pendant allyl groups, providing a robust, facile pendent crosslinking method to control material properties for biomedical applications. As allyl composition controls both the crystallinity and spacing of netpoints, subtle changes in molar composition result in drastic alterations in thermomechanical properties. Molecular weight and gel content can also be adjusted in this copolymerization format to fine-tune material properties. Such a convenient approach can be readily adapted to other promising polymer systems, and bioactive compounds can be incorporated into the crosslinked SMP networks to provide additional functionality. The SMPs possess excellent shape memory properties ($R_f$ and $R_r$ > 98% for most test films) and a suitable range of melting temperatures (43.4 – 29.7 °C) for physiological applications. Films are compliant and ductile with appropriate elastic moduli (70.8 – 2.48 MPa) for vascular applications. Moreover, these SMPs are compatible with vascular endothelial cells (ECs), as indicated *in vitro* by high levels of cell viability (• 85% after after 91 hours relative to TCPS) and healthy cell morphologies. A copolymer construct exhibited successful cellularization without inflammatory exacerbation in a murine model of hindlimb ischemia, indicating the promise of vascular compatibility *in vivo*.

Switch-like shape responses near body temperature, tunable mechanical properties, hydrolytic degradability and vascular compatibility of x%PCL-y%ACPCL copolymers indicate a promising material for constructing stents, vascular grafts, and other medical devices. However, further studies are required before any of this translational potential can be realized. While preliminary short-term results suggest vascular compatibility, a long-term examination of *in vivo* biocompatibility and biodegradability with relevant controls and endpoints is required to adequately ensure the absence of strong host inflammatory reactions to x%PCL-y%ACPCL copolymers and its degradation products [36]. Hemocompatibility tests to assess thrombotic risks from these materials are mandatory. Scalable fabrication techniques, packaging and storage requirements, and other additional testing requirements specific to the type of device desired would also need to be determined. For example, stents comprised of an x%PCL-y%ACPCL copolymer would also require a rational determination of device surface area and surface roughness and evaluation of radial expansion forces, pressure test ratings, fatigue, hysteresis, and radio opacity [16, 32, 71, 83].

Another critical element that needs to be addressed for the ultimate utilization of these x %PCL-y%ACPCL copolymers in minimally-invasive applications is the demonstration of their deployment and recovery from minimally-invasive devices [84]. Depending on whether immediate or delayed onset of actuation is desired in the minimally-invasive surgical procedure and the mechanical requirements of the particular application, the physicochemical properties (i.e. molar composition, molecular weight, and gel content) of the material can be adjusted such that the implant recovers its original device-specific shape at body temperature or slightly above it via very mild resistive heating. In the latter scenario, safe and consistent supplemental heating requirements and methods would need to be determined that achieve sufficient, reliable shape recovery. Direct heating or more nuanced localized heating techniques involving ultrasound [85], magnetic fields [3, 86], electrical currents [4, 87], or photothermal activation [88-92] have all been utilized towards this end.

However, these latter three modes may require incorporation of magnetic nanoparticles (e.g. iron oxide), conductive materials (e.g. carbon nanotubes), or light absorbers (e.g. graphene, gold nanorods, metal complexes, carbon nanotubes, or organic dyes) [9] to produce enough heat for full shape recovery.

The readily-tunable, combinatorial nature of this SMP library provides a unique platform to elucidate unknown structure-function relationships to advance biomaterial and SMP fabrication techniques and optimize material properties for a particular application. A rationale optimization approach would involve 1) first defining the ideal outcome from administering the device (e.g. maximized radial expansion and endothelialization with minimal platelet adhesion to achieve long-term patency with no thrombotic events from stent implantation), 2) hypothesizing the ideal material characteristics to achieve these functional goals (e.g. stiffer material with enhanced surface roughness), and 3) carrying out all tests required for the specific application. 4) Examination of other studies, modeling approaches such as finite element analysis depicting the characteristic equations that determine the functional or material properties, and covariance or principle component analysis could aid in determining the physicochemical properties (e.g. molar composition, molecular weight, crosslinking density, surface roughness, surface area) that generate the desired material or functional properties. If necessary or desired, the existing x%PCL-y %ACPCL copolymer library can be iteratively expanded upon to more precisely elucidate these relationships. Future studies can examine the adaptability of this unique material design involving pendant allyl crosslinkers to other polymer systems, as well as the effects of incorporating bioactive molecules. This may be desired to achieve material and functional properties that cannot be achieved within this x%PCL-y%ACPCL copolymer library for other biomedical, aeronautical, or industrial applications.

## Supplementary Material

Refer to Web version on PubMed Central for supplementary material.

## Acknowledgements

This study was supported by NSF CAREER CBET 1056046 and NSF DMR 1006558. Confocal images were performed in part through the use of the VUMC Cell Imaging Shared Resource (supported by NIH grants CA68485, DK20593, DK58404, HD15052, DK59637 and EY08126). $^{1}$H-NMR was conducted in the Small Molecule NMR Facility Core, and the Translational Pathology Shared Resources Core assisted in the preparation and staining of histological specimens. The authors would also like to acknowledge Mr. Joshua M. Stewart, James Taylor, and Krystian A. Kozek for their assistance in chemical synthesis.

## References

1. Lendlein A, Kelch S. Shape-Memory Polymers. Angewandte Chemie International Edition. 2002; 41:2034–57.
2. Lendlein A, Jiang H, Jünger O, Langer R. Light-induced shape-memory polymers. Nature. 2005; 434:879–82. [PubMed: 15829960]
3. Schmidt AM. Electromagnetic activation of shape memory polymer networks containing magnetic nanoparticles. Macromolecular Rapid Communications. 2006; 27:1168–72.
4. Sahoo NG, Jung YC, Cho JW. Electroactive shape memory effect of polyurethane composites filled with carbon nanotubes and conducting polymer. Materials and Manufacturing Processes. 2007; 22:419–23.

5. Mendez J, Annamalai PK, Eichhorn SJ, Rusli R, Rowan SJ, Foster EJ, et al. Bioinspired mechanically adaptive polymer nanocomposites with water-activated shape-memory effect. Macromolecules. 2011; 44:6827–35.
6. Han XJ, Dong ZQ, Fan MM, Liu Y, Wang YF, Yuan QJ, et al. pH-Induced Shape-Memory Polymers. Macromolecular Rapid Communications. 2012; 33:1055–60. [PubMed: 22517685]
7. Sun L, Huang WM, Ding Z, Zhao Y, Wang CC, Purnawali H, et al. Stimulus-responsive shape memory materials: a review. Materials & Design. 2012; 33:577–640.
8. Hu J, Zhu Y, Huang H, Lu J. Recent advances in shape–memory polymers: Structure, mechanism, functionality, modeling and applications. Progress in Polymer Science. 2012; 37:1720–63.
9. Berg GJ, McBride MK, Wang C, Bowman CN. New directions in the chemistry of shape memory polymers. Polymer. 2014; 55:5849–72.
10. Julich-Gruner KK, Löwenberg C, Neffe AT, Behl M, Lendlein A. Recent Trends in the Chemistry of Shape-Memory Polymers. Macromolecular Chemistry and Physics. 2013; 214:527–36.
11. Liu C, Qin H, Mather P. Review of progress in shape-memory polymers. Journal of materials chemistry. 2007; 17:1543–58.
12. Pretsch T. Review on the Functional Determinants and Durability of Shape Memory Polymers. Polymers. 2010; 2:120–58.
13. Small W, Singhal P, Wilson TS, Maitland DJ. Biomedical applications of thermally activated shape memory polymers. Journal of materials chemistry. 2010; 20:3356–66. [PubMed: 21258605]
14. Serrano MC, Ameer GA. Recent Insights Into the Biomedical Applications of Shape-memory Polymers. Macromolecular bioscience. 2012; 12:1156–71. [PubMed: 22887759]
15. Lendlein A, Behl M, Hiebl B, Wischke C. Shape-memory polymers as a technology platform for biomedical applications. Expert Review of Medical Devices. 2010; 7:357–79. [PubMed: 20420558]
16. Xue L, Dai S, Li Z. Biodegradable shape-memory block co-polymers for fast self-expandable stents. Biomaterials. 2010; 31:8132–40. [PubMed: 20723973]
17. Yakacki CM, Shandas R, Lanning C, Rech B, Eckstein A, Gall K. Unconstrained recovery characterization of shape-memory polymer networks for cardiovascular applications. Biomaterials. 2007; 28:2255–63. [PubMed: 17296222]
18. Ortega J, Maitland D, Wilson T, Tsai W, Sava Ö , Saloner D. Vascular dynamics of a shape memory polymer foam aneurysm treatment technique. Annals of biomedical engineering. 2007; 35:1870–84. [PubMed: 17676399]
19. Maitland DJ, Small W, Ortega JM, Buckley PR, Rodriguez J, Hartman J, et al. Prototype laser-activated shape memory polymer foam device for embolic treatment of aneurysms. Journal of biomedical optics. 2007; 12:030504–-3. [PubMed: 17614707]
20. Small W, Buckley PR, Wilson TS, Benett WJ, Hartman J, Saloner D, et al. Shape memory polymer stent with expandable foam: a new concept for endovascular embolization of fusiform aneurysms. Biomedical Engineering, IEEE Transactions on. 2007; 54:1157–60.
21. McGinn JT, Usman S, Lapierre H, Pothula VR, Mesana TG, Ruel M. Minimally Invasive Coronary Artery Bypass Grafting: Dual-Center Experience in 450 Consecutive Patients. Circulation. 2009; 120:S78–S84. [PubMed: 19752390]
22. Small W IV, Wilson T, Benett W, Loge J, Maitland D. Laser-activated shape memory polymer intravascular thrombectomy device. Optics Express. 2005; 13:8204–13. [PubMed: 19498850]
23. Maitland DJ, Metzger MF, Schumann D, Lee A, Wilson TS. Photothermal properties of shape memory polymer micro-actuators for treating stroke*. Lasers in Surgery and Medicine. 2002; 30:1–11. [PubMed: 11857597]
24. Metzger MF, Wilson TS, Schumann D, Matthews DL, Maitland DJ. Mechanical properties of mechanical actuator for treating ischemic stroke. Biomedical Microdevices. 2002; 4:89–96.
25. Rachev A, Felden L, Ku DN. Design and fabrication of a mechanically matched vascular graft. Journal of biomechanical engineering. 2011; 133:091004. [PubMed: 22010739]
26. Trubel W, Schima H, Moritz A, Raderer F, Windisch A, Ullrich R, et al. Compliance mismatch and formation of distal anastomotic intimal hyperplasia in externally stiffened and lumen-adapted venous grafts. European Journal of Vascular and Endovascular Surgery. 1995; 10:415–23. [PubMed: 7489209]

27. Abbott WM, Megerman J, Hasson JE, L'Italien G, Warnock DF. Effect of compliance mismatch on vascular graft patency. Journal of Vascular Surgery. 1987; 5:376–82. [PubMed: 3102762]
28. Safranski DL, Smith KE, Gall K. Mechanical Requirements of Shape-Memory Polymers in Biomedical Devices. Polymer Reviews. 2013; 53:76–91.
29. Paterson-Brown S, Cheslyn-Curtis S, Biglin J, Dye J, Easmon CS, Dudley HA. Suture materials in contaminated wounds: a detailed comparison of a new suture with those currently in use. The British journal of surgery. 1987; 74:734–5. [PubMed: 2820538]
30. Bunt T, Haynes J. Synthetic vascular graft infection. The continuing headache. Am Surg. 1984; 50:43. [PubMed: 6691635]
31. Bunt T. Vascular graft infections: an update. Cardiovascular Surgery. 2001; 9:225–33. [PubMed: 11336845]
32. Xue L, Dai S, Li Z. Synthesis and characterization of elastic star shape-memory polymers as self-expandable drug-eluting stents. Journal of materials chemistry. 2012; 22:7403–11.
33. Ebara M, Uto K, Idota N, Hoffman JM, Aoyagi T. Shape-Memory Surface with Dynamically Tunable Nano-Geometry Activated by Body Heat. Advanced Materials. 2012; 24:273–8. [PubMed: 21954058]
34. Shih CC, Lin SJ, Chen YL, Su YY, Lai ST, Wu GJ, et al. The cytotoxicity of corrosion products of nitinol stent wire on cultured smooth muscle cells. Journal of biomedical materials research. 2000; 52:395–403. [PubMed: 10951381]
35. Serrano M, Pagani R, Vallet-Regı M, Pena J, Ramila A, Izquierdo I, et al. In vitro biocompatibility assessment of poly (< i> </i>-caprolactone) films using L929 mouse fibroblasts. Biomaterials. 2004; 25:5603–11. [PubMed: 15159076]
36. Filion TM, Xu J, Prasad ML, Song J. In vivo tissue responses to thermal-responsive shape memory polymer nanocomposites. Biomaterials. 2011; 32:985–91. [PubMed: 21040968]
37. Ratna D, Karger-Kocsis J. Recent advances in shape memory polymers and composites: a review. Journal of Materials Science. 2008; 43:254–69.
38. Lendlein A, Schmidt AM, Schroeter M, Langer R. Shape-memory polymer networks from oligo (•-caprolactone) dimethacrylates. Journal of Polymer Science Part A: Polymer Chemistry. 2005; 43:1369–81.
39. Rousseau IA. Challenges of shape memory polymers: A review of the progress toward overcoming SMP's limitations. Polymer Engineering & Science. 2008; 48:2075–89.
40. Lendlein A, Langer R. Biodegradable, elastic shape-memory polymers for potential biomedical applications. Science. 2002; 296:1673–6. [PubMed: 11976407]
41. Garle A, Kong S, Ojha U, Budhlall BM. Thermoresponsive Semicrystalline Poly (- caprolactone) Networks: Exploiting Cross-linking with Cinnamoyl Moieties to Design Polymers with Tunable Shape Memory. ACS applied materials & interfaces. 2012; 4:645–57. [PubMed: 22252722]
42. Nair DP, Cramer NB, Scott TF, Bowman CN, Shandas R. Photopolymerized thiol-ene systems as shape memory polymers. Polymer. 2010; 51:4383–9. [PubMed: 21072253]
43. Nair DP, Cramer NB, McBride MK, Gaipa JC, Shandas R, Bowman CN. Enhanced two-stage reactive polymer network forming systems. Polymer. 2012; 53:2429–34. [PubMed: 22798700]
44. Uygun M, Tasdelen MA, Yagci Y. Influence of type of initiation on thiol–ene “click” chemistry. Macromolecular Chemistry and Physics. 2010; 211:103–10.
45. Nair DP, Podgórski M, Chatani S, Gong T, Xi W, Fenoli CR, et al. The Thiol-Michael Addition Click Reaction: A Powerful and Widely Used Tool in Materials Chemistry. Chemistry of Materials. 2013; 26:724–44.
46. Xu X, Davis KA, Yang P, Gu X, Henderson JH, Mather PT. Shape Memory RGD-Containing Networks: Synthesis, Characterization, and Application in Cell Culture. Macromolecular Symposia: Wiley Online Library. 2011:162–72.
47. Wang X, Boire TC, Bronikowski C, Zachman AL, Crowder SW, Sung H-J. Decoupling polymer properties to elucidate mechanisms governing cell behavior. Tissue Engineering Part B: Reviews. 2012; 18:396–404. [PubMed: 22536977]
48. Woodruff MA, Hutmacher DW. The return of a forgotten polymer—polycaprolactone in the 21st century. Progress in Polymer Science. 2010; 35:1217–56.

49. Jeong H, Kim B, Choi Y. Synthesis and properties of thermotropic liquid crystalline polyurethane elastomers. Polymer. 2000; 41:1849–55.
50. Bothe M, Mya KY, Lin EMJ, Yeo CC, Lu X, He C, et al. Triple-shape properties of star-shaped POSS-polycaprolactone polyurethane networks. Soft Matter. 2012; 8:965–72.
51. Luo H, Liu Y, Yu Z, Zhang S, Li B. Novel Biodegradable Shape Memory Material Based on Partial Inclusion Complex Formation between -Cyclodextrin and Poly(•-caprolactone). Biomacromolecules. 2008; 9:2573–7. [PubMed: 18798668]
52. Messori M, Degli Esposti M, Paderni K, Pandini S, Passera S, Riccò T, et al. Chemical and thermomechanical tailoring of the shape memory effect in poly( -caprolactone)-based systems. Journal of Materials Science. 2013; 48:424–40.
53. Mya KY, Gose HB, Pretsch T, Bothe M, He C. Star-shaped POSS-polycaprolactone polyurethanes and their shape memory performance. Journal of materials chemistry. 2011; 21:4827–36.
54. Neuss S, Blomenkamp I, Stainforth R, Boltersdorf D, Jansen M, Butz N, et al. The use of a shape-memory poly( -caprolactone)dimethacrylate network as a tissue engineering scaffold. Biomaterials. 2009; 30:1697–705. [PubMed: 19121539]
55. Mani G, Feldman MD, Patel D, Agrawal C. Coronary stents: a materials perspective. Biomaterials. 2007; 28:1689–710. [PubMed: 17188349]
56. Parrish B, Quansah JK, Emrick T. Functional polyesters prepared by polymerization of -allyl (valerolactone) and its copolymerization with -caprolactone and -valerolactone. Journal of Polymer Science Part A: Polymer Chemistry. 2002; 40:1983–90.
57. Mahmud A, Xiong X-B, Lavasanifar A. Novel Self-Associating Poly (ethylene oxide)-b lock-poly ( -caprolactone) Block Copolymers with Functional Side Groups on the Polyester Block for Drug Delivery. Macromolecules. 2006; 39:9419–28.
58. Molander GA, Harris CR. Sequenced reactions with samarium (II) iodide. Tandem intramolecular nucleophilic acyl substitution/intramolecular Barbier cyclizations. Journal of the American Chemical Society. 1995; 117:3705–16.
59. Darcos V, Antoniacomi S, Paniagua C, Coudane J. Cationic polyesters bearing pendent amino groups prepared by thiol–ene chemistry. Polymer Chemistry. 2012; 3:362–8.
60. Pitt CG, Chasalow F, Hibionada Y, Klimas D, Schindler A. Aliphatic polyesters. I. The degradation of poly (•-caprolactone) in vivo. Journal of Applied Polymer Science. 1981; 26:3779–87.
61. Guo B, Chen Y, Lei Y, Zhang L, Zhou WY, Rabie ABM, et al. Biobased poly (propylene sebacate) as shape memory polymer with tunable switching temperature for potential biomedical applications. Biomacromolecules. 2011; 12:1312–21. [PubMed: 21381645]
62. Defize T, Riva R, Raquez J-M, Dubois P, Jérôme C, Alexandre M. Thermoreversibly Crosslinked Poly( -caprolactone) as Recyclable Shape-Memory Polymer Network. Macromolecular Rapid Communications. 2011; 32:1264–9. [PubMed: 21692124]
63. Wagermaier, W.; Kratz, K.; Heuchel, M.; Lendlein, A. Characterization Methods for Shape-Memory Polymers.. In: Lendlein, A., editor. Shape-Memory Polymers. Springer; Berlin Heidelberg: 2010. p. 97-145.
64. Lancaster MV, Fields RD. Microbiocides and conversion of resazurin to resorfurin. Google Patents. 1996
65. Niiyama H, Huang NF, Rollins MD, Cooke JP. Murine Model of Hindlimb Ischemia. 2009:e1035.
66. Couffinhal T, Silver M, Zheng LP, Kearney M, Witzenbichler B, Isner JM. Mouse model of angiogenesis. The American Journal of Pathology. 1998; 152:1667–79. [PubMed: 9626071]
67. Zachman AL, Wang X, Tucker-Schwartz JM, Fitzpatrick ST, Lee SH, Guelcher SA, et al. Uncoupling angiogenesis and inflammation in peripheral artery disease with therapeutic peptide-loaded microgels. Biomaterials. 2014; 35:9635–48. [PubMed: 25154665]
68. Hu X, Chen X, Liu S, Shi Q, Jing X. Novel aliphatic poly (ester-carbonate) with pendant allyl ester groups and its folic acid functionalization. Journal of Polymer Science Part A: Polymer Chemistry. 2008; 46:1852–61.
69. Karikari AS, Edwards WF, Mecham JB, Long TE. Influence of peripheral hydrogen bonding on the mechanical properties of photo-cross-linked star-shaped poly (D, L-lactide) networks. Biomacromolecules. 2005; 6:2866–74. [PubMed: 16153129]

70. Xue L, Dai S, Li Z. Synthesis and Characterization of Three-Arm Poly ( -caprolactone)-Based Poly (ester–urethanes) with Shape-Memory Effect at Body Temperature. Macromolecules. 2009; 42:964–72.
71. Yakacki CM, Shandas R, Lanning C, Rech B, Eckstein A, Gall K. Unconstrained recovery characterization of shape-memory polymer networks for cardiovascular applications. Biomaterials. 2007; 28:2255–63. [PubMed: 17296222]
72. Zhu G, Liang G, Xu Q, Yu Q. Shape-memory effects of radiation crosslinked poly (•-caprolactone). Journal of Applied Polymer Science. 2003; 90:1589–95.
73. Li F, Zhu W, Zhang X, Zhao C, Xu M. Shape memory effect of ethylene–vinyl acetate copolymers. Journal of Applied Polymer Science. 1999; 71:1063–70.
74. Karimi A, Navidbakhsh M, Shojaei A, Faghihi S. Measurement of the uniaxial mechanical properties of healthy and atherosclerotic human coronary arteries. Materials Science and Engineering: C. 2013; 33:2550–4. [PubMed: 23623067]
75. Ota S. Current status of irradiated heat-shrinkable tubing in Japan. Radiation Physics and Chemistry (1977). 1981; 18:81–7.
76. Kleinheins G, Starkl W, Nuffer K. Special features of quality assurance measures for radiation-cured, heat-shrunk products. 1984
77. Kleinhans G, Heidenhain F. Actively moving polymers. Kunststoffe. 1986; 76:1069–73.
78. Feldkamp DM, Rousseau IA. Effect of the Deformation Temperature on the Shape-Memory Behavior of Epoxy Networks. Macromolecular Materials and Engineering. 2010; 295:726–34.
79. Gall K, Yakacki CM, Liu Y, Shandas R, Willett N, Anseth KS. Thermomechanics of the shape memory effect in polymers for biomedical applications. Journal of Biomedical Materials Research Part A. 2005; 73:339–48. [PubMed: 15806564]
80. McClung AJ, Tandon GP, Baur JW. Deformation rate-, hold time-, and cycle-dependent shape-memory performance of Veriflex-E resin. Mechanics of Time-Dependent Materials. 2013; 17:39–52.
81. Lam CX, Hutmacher DW, Schantz JT, Woodruff MA, Teoh SH. Evaluation of polycaprolactone scaffold degradation for 6 months in vitro and in vivo. Journal of Biomedical Materials Research Part A. 2009; 90:906–19. [PubMed: 18646204]
82. Maciaq TKJ, Wilkins L, Stemerman MB, Weinstein R. Organizational behavior of human umbilical vein endothelial cells. The Journal of cell biology. 1982; 94:511–20. [PubMed: 6813338]
83. Yang C-S, Wu H-C, Sun J-S, Hsiao H-M, Wang T-W. Thermo-Induced Shape-Memory PEG-PCL Copolymer as a Dual-Drug-Eluting Biodegradable Stent. ACS applied materials & interfaces. 2013; 5:10985–94. [PubMed: 24111673]
84. Kratz K, Voigt U, Lendlein A. Temperature-Memory Effect of Copolyesterurethanes and their Application Potential in Minimally Invasive Medical Technologies. Advanced Functional Materials. 2012; 22:3057–65.
85. Li G, Fei G, Xia H, Han J, Zhao Y. Spatial and temporal control of shape memory polymers and simultaneous drug release using high intensity focused ultrasound. Journal of materials chemistry. 2012; 22:7692–6.
86. Yang D, Huang W, He X, Xie M. Electromagnetic activation of a shape memory copolymer matrix incorporating ferromagnetic nanoparticles. Polymer International. 2012; 61:38–42.
87. Fei G, Tuinea-Bobe C, Li D, Li G, Whiteside B, Coates P, et al. Electro-activated surface micropattern tuning for microinjection molded electrically conductive shape memory polyurethane composites. RSC Advances. 2013; 3:24132–9.
88. Hribar KC, Metter RB, Ifkovits JL, Troxler T, Burdick JA. Light-Induced Temperature Transitions in Biodegradable Polymer and Nanorod Composites. Small. 2009; 5:1830–4. [PubMed: 19408258]
89. Liu Y, Boyles JK, Genzer J, Dickey MD. Self-folding of polymer sheets using local light absorption. Soft Matter. 2012; 8:1764–9.
90. Liu Y, Miskiewicz M, Escuti MJ, Genzer J, Dickey MD. Three-dimensional folding of pre-strained polymer sheets via absorption of laser light. Journal of Applied Physics. 2014; 115:204911.

91. Zhang H, Zhang J, Tong X, Ma D, Zhao Y. Light Polarization-Controlled Shape-Memory Polymer/Gold Nanorod Composite. Macromolecular Rapid Communications. 2013; 34:1575–9. [PubMed: 24092559]

92. Zhang H, Zhao Y. Polymers with Dual Light-Triggered Functions of Shape Memory and Healing Using Gold Nanoparticles. ACS applied materials & interfaces. 2013; 5:13069–75. [PubMed: 24308556]

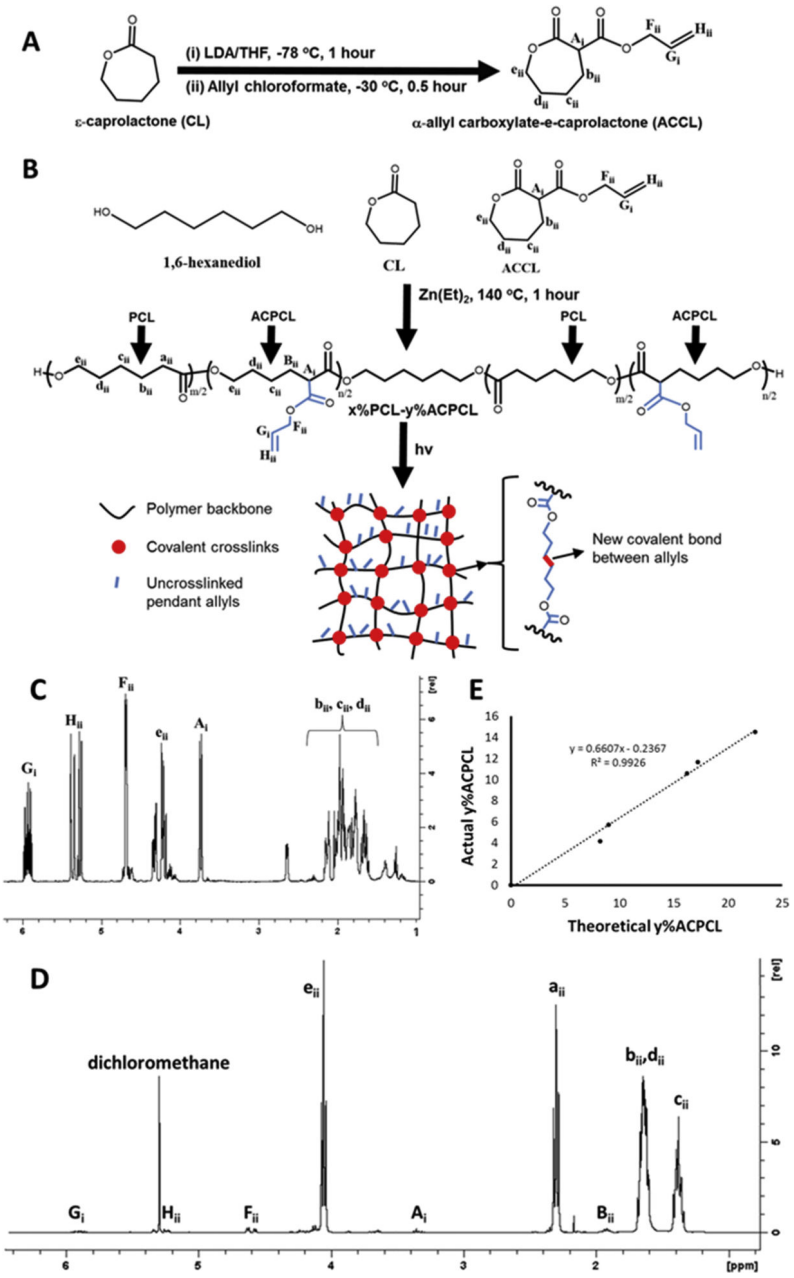


**Figure 1.**

(A) Synthetic scheme for ACCL and (B) x%PCL-y%ACPCL SMP networks. (C) $^{1}$HNMR of ACCL (400 MHz, $CDCl_3$, 25 °C, TMS): δ = 5.92 (m, 1H;, -C**H**=$CH_2$ (***G*****$_i$**)), 5.31 (m, 2H; -CH=C**H**$_2$ (***H*****$_{ii}$**)), 4.63 (m, 2H; -CH=CC**H**$_2$O (***F*****$_{ii}$**)), 4.20 (m, 2H; -OC**H**$_2$ (***e*****$_{ii}$**)), 3.73 (d, $^{3}$J(H,H) = 10.7 Hz, 1H; -C**H**$CH_2CH_2$ (***A*****$_i$**)), 2.40 – 1.50 (m, 6H; -C**H**$_2$ (***b*****$_{ii}$**,***c*****$_{ii}$**,***d*****$_{ii}$**)). (D) $^{1}$H-NMR of 96%PCL-04%ACPCL (400 MHz, $CDCl_3$, 25 °C, TMS): δ = 5.92 (m, 1H;, -C**H**=$CH_2$ (***G*****$_i$**)), 5.31 (m, 2H; -CH=C**H**$_2$ (***H*****$_{ii}$**)), 4.63 (m, 2H; -CH=C**H**$_2$O (***F*****$_{ii}$**)), 4.15 (m, 2H; -OC**H**$_2$ (***e*****$_{ii}$**)), 3.35 (m, 1H; -C**H**$CH_2$ (***A*****$_i$**)), 2.33 (t, $^{3}$J(H,H) = 7.5 Hz, 2H; -C**H**$_2$ (***a*****$_{ii}$**)), 1.96 (m, 2H; -C**H**$_2$ (***B*****$_{ii}$**)), 1.62 (m, 4H; -C**H**$_2$ (***b*****$_{ii}$**,***d*****$_{ii}$**)), 1.39 ppm (m, 2H; -C**H**$_2$ (***c*****$_{ii}$**)). (E) Influence of ACCL:CL feed ratio on x%PCL-y%ACPCL molar composition

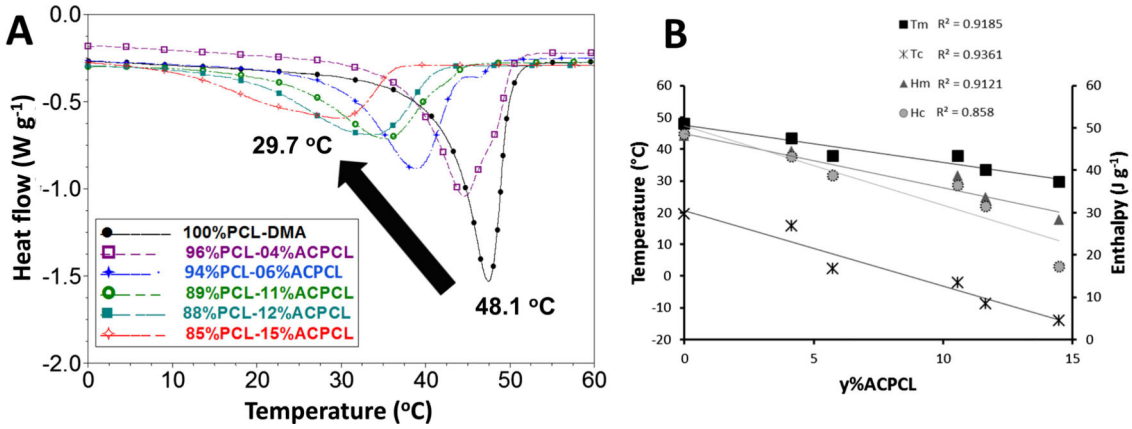


**Figure 2.**

(A) DSC overlay and (B) correlation between y%ACPCL and thermal properties for crosslinked x%PCL-y%ACPCL SMP networks.

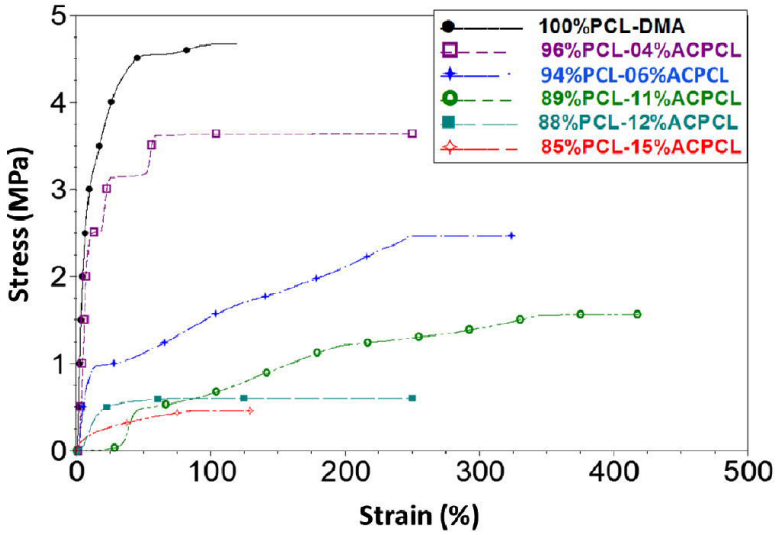


**Figure 3.**
Stress vs. strain curves for crosslinked x%PCL-y%ACPCL SMP networks at 37 °C.

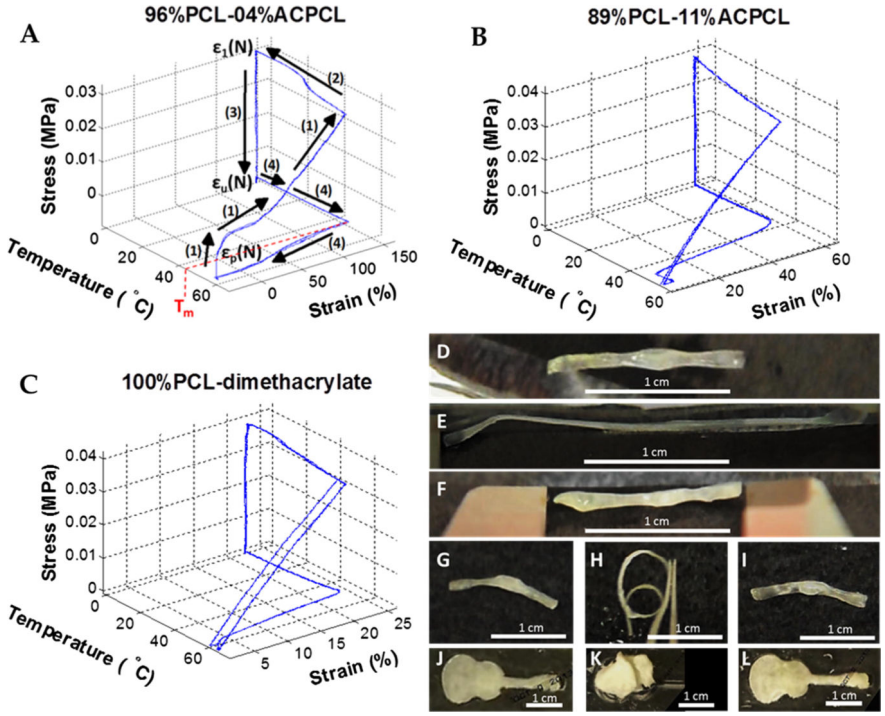


**Figure 4.**

(A-C) Stress-controlled thermomechanical cycling of crosslinked x%PCL-y%ACPCL and 100%PCL-DMA SMP networks. (D-L) Shape memory demonstrations. (D, G) 88%PCL-12%ACPCL tubular permanent shape is (E, H) deformed into a thread by heating at 50 °C, applying strain, and fixing in an ice bath. (F, I) Heating at 37 °C results in recovery of the original, permanent tube shape. (J) 96%PCL-04%ACPCL guitar shape is (K) heated to 50 °C, strained, contorted, and fixed at 4 °C before (L) ultimate recovery of the complex guitar shape at 48 °C.

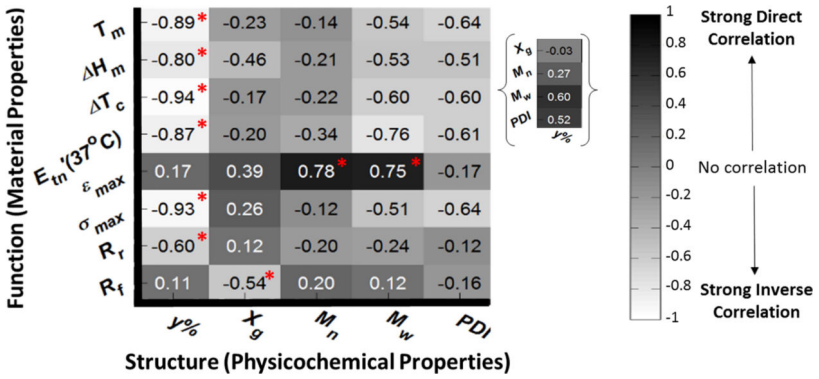


**Figure 5.**

Standardized covariance matrix reveals structure-function relationships for the crosslinked SMP library. * does not indicate statistical significance, but rather the strongest Structural/Physicochemical Property correlation(s) with each Functional/Material Property. Molar composition (y%) has the strongest influence on the majority of material properties. The inset showing the correlation of y% with the other physicochemical properties provides context (i.e. interdependence information) for the structure-function relationships generated from the SMP library.

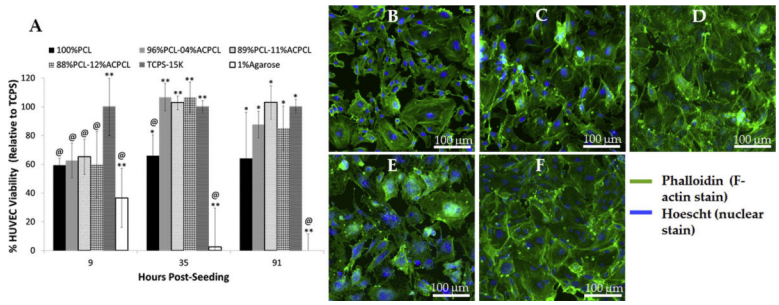


**Figure 6.**

(A) Viability of HUVECs seeded directly on polymer surfaces at specified timepoints, where @ = significantly different from TCPS, * = significantly different from 1% agarose, and ** = significantly different from 100%PCL as well as 1% agarose (if located above the 1% agarose bar, the only significant difference is to 100%PCL) ($n = 4$, $p < 0.05$). Confocal microscopy images of human coronary artery endothelial cells (hCAECs) 3 days post-seeding on (B) TCPS, (C) 100%PCL, (D) 96%PCL-04%ACPCL, (E) 89%PCL-11%ACPCL, and (F) 88%PCL-12%ACPCL exhibit trademark cobblestone morphology (Green: F-actin, Blue: Nuclei).

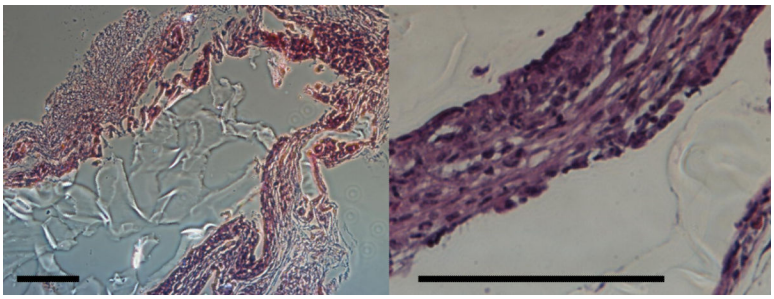

**Figure 7.**

H&E Staining of *in vivo* biocompatibility study illustrates the tubular SMP construct implanted into the thigh muscle adjacent to the femoral artery ligations in a mouse model of hindlimb ischemia. Left (10×) and right (40×); Scale bar = 100 μm.

**Table 1**

Characterization of x%PCL-y%ACPCL copolymers

| Copolymer | Theoretical y (%) | Actual y (%) | Yield (%) | Initiator: Monomer | $M_n$ (Da) | $M_w$ (Da) | PDI | $T_m$ (°C) | $X_C$ (%) |
|---|---|---|---|---|---|---|---|---|---|
| 100%PCL | 0.00 | 0.00 | 86.2 | 1:100 | 11300 | 17368 | 1.54 | 53.0 ± 0.2 | 56.6 ± 1.5 |
| 100%PCL-DMA | 0.00 | 0.00 | N/A | N/A | 11628 | 16417 | 1.41 | 50.7 ± 0.5 | 45.8 ± 1.9 |
| 96%PCL-04%ACPCL | 8.24 | 4.16 | 44.8 | 1:200 | 15060 | 26870 | 1.78 | 45.9 ± 0.3 | 41.6 ± 1.2 |
| 94%PCL-06%ACPCL | 9.03 | 5.74 | 38.3 | 1:200 | 16546 | 39050 | 2.36 | 47.1 ± 0.1 | 36.1 ± 0.5 |
| 89%PCL-11%ACPCL | 16.2 | 10.6 | 39.8 | 1:200 | 13627 | 34049 | 2.50 | 39.1 ± 0.3 | 30.4 ± 0.7 |
| 88%PCL-12%ACPCL | 17.2 | 11.7 | 22.6 | 1:315 | 19087 | 36430 | 1.91 | 41.6 ± 0.2 | 31.1 ± 0.7 |
| 85%PCL-15%ACPCL | 22.5 | 14.5 | 56.6 | 1:200 | 12095 | 28931 | 2.39 | 32.5 ± 0.4 | 24.4 ± 0.9 |

**Table 2**

Gel content and thermal properties of crosslinked x%PCL-y%ACPCL SMP films

| Composition | $X_G$ (%) | $T_m$ (°C) | $\Delta H_m$ (J $g^{-1}$) | $X_C$ (%) | $T_c$ (°C) | $\Delta H_c$ (J $g^{-1}$) | $T_g$ (°C) |
|---|---|---|---|---|---|---|---|
| 100%PCL-DMA | 72.0 ± 17 | 48.1 ± 0.4 | 48.2 ± 0.5 | 34.6 ± 0.4 | 19.5 ± 1.0 | 48.6 ± 0.38 | −54.2 ± 3.0 |
| 96%PCL-04%ACPCL | 63.0 ± 8.6 | 43.4 ± 1.2 | 44.6 ± 3.2 | 32.0 ± 2.3 | 15.8 ± 0.89 | 43.2 ± 6.1 | −56.9 ± 0.10 |
| 94%PCL-06%ACPCL | 60.3 ± 21 | 37.9 ± 0.9 | 39.1 ± 5.3 | 28.0 ± 3.8 | 2.44 ± 0.54 | 38.7 ± 4.8 | −58.8 ± 4.9 |
| 89%PCL-11%ACPCL | 49.0 ± 6.2 | 37.9 ± 0.7 | 38.7 ± 1.6 | 27.7 ± 1.2 | −2.10 ± 0.74 | 36.5 ± 0.82 | −57.1 ± 1.5 |
| 88%PCL-12%ACPCL | 64.1 ± 3.1 | 33.4 ± 1.2 | 33.7 ± 1.1 | 24.2 ± 0.8 | −8.73 ± 0.20 | 31.4 ± 2.2 | −58.7 ± 2.2 |
| 85%PCL-15%ACPCL | 50.3 ± 0.64 | 29.7 ± 0.2 | 28.3 ± 2.7 | 20.3 ± 1.9 | −13.9 ± 0.84 | 17.2 ± 0.87 | −57.5 ± 1.1 |

**Table 3**

Mechanical and shape memory properties of crosslinked SMP films

| Composition | $E_{tn}$(37°C) (MPa) | $\varepsilon_{max}$ (%) | $\sigma_{max}$ (MPa) | $R_r$ (1) (%) | $R_r$ (N) (%) | $R_f$ (N) (%) |
|---|---|---|---|---|---|---|
| 100%PCL-DMA | 66.7 ± 41.6 | 90.2 ± 110 | 3.86 ± 2.2 | 99.7 ± 0.12 | 99.5 ± 1.4 | 98.3 ± 1.5 |
| 96%PCL-04%ACPCL | 70.8 ± 37.4 | 126 ± 115 | 3.15 ± 0.39 | 99.2 ± 0.81[a] | 99.4 ± 1.3[a] | 94.2 ± 1.2[a] |
| 94%PCL-06%ACPCL | 3.05 ± 2.64 | 253 ± 19.4 | 2.36 ± 0.87 | 93.7 ± 0.87 | 98.5 ± 0.57 | 98.7 ± 0.27 |
| 89%PCL-11%ACPCL | 5.44 ± 1.10 | 300 ± 127 | 1.43 ± 0.31 | 97.7 ± 0.62 | 99.7 ± 0.74 | 99.8 ± 0.16 |
| 88%PCL-12%ACPCL | 3.64 ± 1.10 | 109 ± 110 | 1.14 ± 0.59 | 99.3 ± 9.9 | 99.0 ± 6.2 | 98.6 ± 0.75 |
| 85%PCL-15%ACPCL | 2.48 ± 1.11 | 71.5 ± 40.6 | 0.463 ± 0.4 | 60.1 ± 0.64 | 86.9 ± 4.7 | 99.6 ± 0.23 |

[a] A 96%PCL-04%ACPCL test film with $X_G$ = 36.7 ± 8.6% had $R_r$(1) = 99.9 ± 0.2, $R_r$(N) = 99.8 ± 0.4%, and $R_f$(N) = 99.8 ± 0.1%.